ELSEVIER

Contents lists available at ScienceDirect

Progress in Organic Coatings

journal homepage: www.elsevier.com/locate/porgcoat



Effects of NIR-reflective pigments on waterborne polyurethane coatings and their thermal insulation performance

Zichen Ling, Qixin Zhou

Department of Chemical, Biomolecular, and Corrosion Engineering, The University of Akron, Akron, OH 44325, United States

ARTICLE INFO

Keywords: Polyurethane Waterborne NIR reflectance Pigment

ABSTRACT

Waterborne coatings have garnered much attention and gradually occupied the coating market recently due to the significant advantages in volatile organic compound emissions compared with solvent-borne coatings. Waterborne polyurethane coatings are a majority portion of waterborne coatings. Unlike solvent-borne coatings, the film formation of waterborne coatings occurs in an inhomogeneous phase, which brings a challenge for pigmentation in waterborne coatings. However, the influence of pigment on film formation and the property of waterborne polyurethane coating remain unclear. In this study, the different contents of commercial black near-infrared (NIR) reflective pigments were incorporated into both commercial and synthetic waterborne polyurethane systems. The film formation process was monitored by multispeckle diffusing wave spectroscopy. The impact of the pigment content on dry films was assessed through scanning electron microscope, color and gloss measurements, dynamical thermal analyzer, and tensile testing. Furthermore, the thermal insulation performance of the waterborne polyurethane coatings was evaluated to study the function of the NIR reflective pigments. Our findings reveal that the addition of black NIR reflective pigments yields a multifaceted effect on film formation and coating morphology and improves thermal insulating property. Elevated pigment content correlated with increased crosslinking density, tensile stress, and Young's modulus.

1. Introduction

The principle of green chemistry is reducing or eliminating the use of hazardous materials [1]. In the coating industry, two major categories of polymeric coatings are solvent-borne and waterborne, classified by the types of solvent carrier. The evaporation of volatile organic compounds (VOCs) causes flammability and inhalation risk, which violates the green chemistry principle. Also, strict regulations limit the use of VOCs in coatings in many countries [2,3]. Therefore, waterborne coatings have gained favor among customers and manufacturers because of their low VOC emission, low flammability, and other benefits. Nowadays, waterborne coatings are gradually replacing solvent-borne coatings, with the global market projected to reach 140.7 billion dollars by 2030 [41.

Pigments are important ancillary materials in industrial paints that not only introduce color to the binders but also bring other special properties like flame retardant and corrosion resistance [5–9]. Unlike soluble dyes, pigments are insoluble solids and are suspended in binders with unaffected physical and chemical properties. There are two types of

pigments—inorganic pigments and organic pigments. Inorganic pigments contain metal oxide, sulfide, or salt, and organic pigments always contain carbons, along with other elements [10]. Compared with pigments of other colors, black pigments like carbon black absorb visible light (400–700 nm), as well as near-infrared (NIR) light (700–2500 nm) which accounts for approximately 50 % of solar radiation to store heat [11–15]. Black pigments are mainly used in paints for exterior walls and roofs. If a "cool" paint can reflect NIR radiation, it will decrease the absorption of solar energy by buildings and paved surfaces to alleviate the "heat island effect." It is estimated that if the reflectance of a building's roof is increased to 40 %, the electricity used for air conditioning in summer will be reduced by 20–40 % [16]. Therefore, black NIR-reflective pigments are worthy of research and application due to their potential to significantly lower energy consumption.

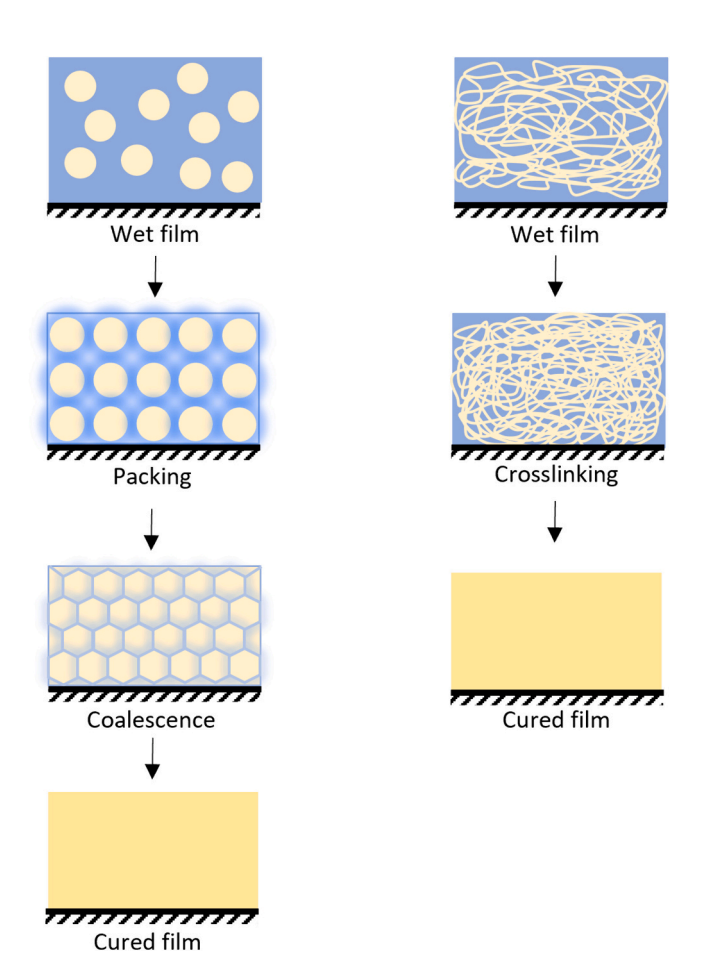
Pigments that have high NIR reflectivity are ideal for these "cool" coatings, as they can provide coatings that are similar in color to conventional pigments but can reflect near-infrared light instead of absorbing it. A bunch of studies have incorporated different black NIR-reflective pigments in the coating system to investigate the coating's

E-mail address: qzhou@uakron.edu (Q. Zhou).

 $^{^{\}ast}$ Corresponding author.

thermal insulating properties. You et al. developed black NIR-reflective coatings by incorporating the CuO nanoparticles into the solvent-borne epoxy binder. The effects of shapes and mass percentages of CuO nanoparticles on the spectral reflectance properties were investigated [17]. Martini et al. compared the crystallinity degree of commercial and synthetic black pigments on the coating thermal insulation behavior in waterborne acrylic coatings [18]. However, these studies mainly focus on the final properties of coatings and the characteristics of NIR-reflective pigments. Rare studies investigated the influences of NIR-reflective pigments on the coating formation process—monitor the coating formation process and link it to the final coating film properties, especially in the context of waterborne coatings.

The film formation process in solvent-borne and waterborne coatings is different. As illustrated in Scheme 1, in a solvent-borne system, most of the solvent evaporates rapidly while the polymer chains entangle with each other and form a solid film. The rest of the solvent will further evaporate through the polymer network over a long period. This process occurs in a uniform and homogeneous phase. In contrast, in a waterborne coating, the prepolymer is kept stable in the aqueous phase by introducing hydrophilic groups. After the application of a waterborne coating, water gradually evaporates, causing the polymer particles to tightly contact and pack as spheres. With further water evaporation, the system's viscosity sharply increases, causing particles to deform into a hexagonal structure. Subsequently, with the coalescence and interdiffusion between polymer particles, a uniform film is formed. Simultaneously, the remaining water in the coating rises to the surface and evaporates [19-21]. Unlike solvent-borne coatings, the film formation of waterborne coatings occurs in an inhomogeneous phase, which makes it possible to leave some defects or voids for waterborne coatings due to



Scheme 1. Film formation of waterborne coating (left) and solvent-borne coating (right).

the air invasion and uncomplete closure of interstices during coating formation [22,23].

Therefore, a substantial opportunity exists for further exploration of the film formation and waterborne coating properties after incorporating the NIR-reflective pigments. Also, based on the research experience in waterborne non-isocyanate polyurethane (WNIPU) development in our research group, it is needed to study the pigmented WNIPU coating to further expand its applications. In general, the propertyprocessing relationship of NIR-reflective pigments in waterborne coatings is worth further understanding, especially in waterborne nonisocyanate polyurethanes. In this study, the commercial NIR-reflective pigments were incorporated into two waterborne polyurethane coatings: one is a commercially used waterborne polyurethane (WPU) and the other is a lab-synthesized WNIPU based on our previous research [24]. Following the application of the coating, the film formation was monitored by multispeckle diffusing wave spectroscopy (MS-DWS). The morphology of the cured films was examined using a scanning electron microscope (SEM). Additionally, the properties including glass transition temperature and tensile properties were characterized by a dynamical thermal analyzer (DMTA) and tensile test, respectively. The impact of film formation on the coating properties was delved. Furthermore, the thermal insulation performance of WPU films was assessed using a thermal camera.

2. Experimental

2.1. Materials

The copper chromite black spinel pigment (HEUCODUR® Black 9-100) was generously provided by Heubach (Germany). The commercial WPU (Varathane 200241H Water-Based Ultimate Polyurethane) was purchased from Amazon. 3,3'-diamino-N-methyldipropyl-amine (DMDPA, 96 %, 145.25 g mol $^{-1}$), tetrabutylammonium bromide (TBAB, \geq 98 %), bisphenol A diglycidyl ether (DGEBA, 340.41 g mol $^{-1}$), and acetic acid (\geq 99.7 %) were purchased from Sigma-Aldrich. Ethanol (200 proof) was purchased from Fisher Scientific. PRIAMINE 1075-LQ (GD) dimer fatty acid diamine (FDA) was kindly provided by CRODA (UK). All materials were used as received without further purification.

2.2. Synthesis of waterborne non-isocyanate polyurethane (WNIPU)

The synthesis of WNIPU was based on our previous report [24]. In summary, 150.0 g of DGEBA was firstly subjected to a reaction with $\rm CO_2$ catalyzed by 5.0 g TBAB at 130 °C for 96 h, yielding the DGEBA-based cyclic carbonate. Secondly, 15.0 g DGEBA cyclic carbonate, 5.0 g DMDPA, and 18.5 g fatty acid diamine were mixed in ethanol under $\rm N_2$ atmosphere and heated to 75 °C for 8 h to produce the amine-terminated NIPU. After cooling to room temperature, 23.0 g DGEBA was added to the mixture and stirred for 1 h. Then, an equivalent amount of acetic acid based on the quantity of DMDPA was added to the mixture to neutralize the product under stirring for 1 h. Here the molar ratio of the cyclic carbonate group/epoxy group/amine group was 1:1:2. Finally, the NIPU polymer was dispersed in deionized water, followed by solvent removal using a rotary evaporator. The solid content of the waterborne NIPU was 27.4 wt%, identical to that of the commercial WPU.

2.3. Dispersion of NIR-reflective pigments in waterborne polyurethane coating

To prepare the pigmentated waterborne coating dispersion, the corresponding amount of pigment was added to the waterborne polyurethane coating and mixed using the ultrasonic processors (Cole-Parmer, IL, US) for 10 min. The pigmented coating formulation is listed in Table 1 and each formulation is named according to the type of coatings and the pigment content. For instance, 'WPU-1' denotes the commercial WPU containing 1 wt% of pigment, while 'WNIPU-1'

Table 1The coating formulation and its characteristic values (wt%).

Water content
72.6
71.9
69.0
65.3
58.1
72.6
71.9
69.0
65.3
58.1

represents the synthesized WNIPU with 1 wt% of pigment. The pigment content was determined based on the total weight of the dispersion. Due to the addition of pigment, the solid content and water content in the waterborne coating were recalculated, as indicated in Table 1.

2.4. Coating application

After the pigment dispersion, the waterborne polyurethane coatings were applied on the QD-36 steel panels (Q-Lab Corporation) using a drawdown bar with a wet film thickness of 150 μ m. The touch-free films were obtained within 1 h. Subsequently, the samples were left at room temperature for 7 days to allow the formation of mechanically robust dry films with a thickness of 45 μ m.

2.5. Characterization

The film formation process was monitored by the CurinScan optical film formation analyzer, which is based on the multispeckle diffusing wave spectroscopy (MS-DWS). The testing was conducted by FOR-MULACTION Scientific Instruments (OH, US) [24,25]. This testing was performed on the waterborne coatings applied to the QD-36 panels, with a wet film thickness of 150 μm .

The morphology of the pigment was characterized by the transmission electron microscope (TEM, Tecnai G2 F20) at 200 kV. The dry coating films were captured by the scanning electron microscope (SEM, Hitachi S-2600 N) at 5 kV.

Thermogravimetric analysis (TGA) was performed using a TA Instruments Q500. 10 mg samples were heated to 600 $^{\circ}\text{C}$ at a steady rate of $10~^{\circ}\text{C}$ min $^{-1}$ under a nitrogen atmosphere (10 ml min $^{-1}$) and maintained at 600 $^{\circ}\text{C}$ for 10 min.

The viscoelastic properties of the coating films were assessed by the dynamical thermal analyzer (DMTA, Q800, TA Instruments) in tension mode, with a constant frequency of 1 Hz. Self-standing films were peeled from the substrates and cut to approximately 15 mm in length and 10 mm in width. The samples were cooled to $-30\,^{\circ}\text{C}$ and heated to 150 $^{\circ}\text{C}$ at a rate of 3 $^{\circ}\text{C}$ min $^{-1}$.

Tensile testing was carried out with an Instron 5567 testing machine (Instron Corp) at room temperature, with a moving speed of 5 mm $\rm min^{-1}$. Self-standing films were peeled from the substrates and cut to approximately 30 mm in length and 10 mm in width. Average data were obtained from five duplicable tests for each sample.

The CIELAB values and 60° gloss of waterborne coating films were measured by the color & gloss meter (BYK, Wesel, Germany). The reported results represent the average values obtained from 5 different spots on the films.

3. Results and discussion

3.1. Drying kinetics of the waterborne polyurethane coatings

MS-DWS is an effective method for monitoring the drying process and determining the critical time for each stage during curing. The

testing procedure involves a laser illuminating the sample, with photons being backscattered by the materials within the sample. These backscattered photons are then detected by a video camera and presented as an interference image, referred to as a 'Speckle image'. As film formation occurs, the motion speed of scatters within the sample changes, thereby affecting the intensity fluctuations in the speckle image. Through the monitoring and analysis of variations in the speckle image, the dynamics of particles or structural changes could be obtained during the curing process [25,26].

Fig. 1 displays the micro-dynamic (mD) behavior of the commercial WPU as the function of time, while the results of synthetic WNIPU can be found in Fig. S1. The stage preceding involves water evaporation and the packing of the prepolymer. As the particles draw closer with the evaporation of water, the collision of particles leads to variation in mD [27]. The critical time characterized as the end of this stage is defined as t_{c1}. Subsequently, the coalescence stage involves further water evaporation, packing, and interdiffusion of the prepolymer, resulting in the formation of the cured film, with t_{c2} representing the end of this stage. The critical times (t_{c1} and t_{c2}) for each sample are listed in Table 2. The results indicate that both t_{c1} and t_{c2} slightly decrease with the addition of the pigment and then gradually increase with further increasing of pigment. For instance, t_{c1} steadily decreases from 24 min (WPU-0) to 20 min (WPU-5), after which it increases to 26 min (WPU-20), exceeding the value for the neat sample, and tc2 behaves similarly, from 35 min (WPU-0) decreases to 34 min (WPU-5) then increases to 54 min (WPU-20). Initially, the addition of the pigment increases the solid content, facilitating particle packing and water evaporation. However, with a further increase in the pigment content, the upper layer of the wet coat dries rapidly, impeding dissipation within the coating. Consequently, the system maintains high mobility for a period due to the extended drying time. The pigmented WNIPU coating demonstrated a similar drying and curing trend to that in WPU coating, and the influence of the pigments on drying time is more significant than that in WPU. The tc_1 drops from 28 min (WNIPU-0) to 11 min (WNIPU-1), then increases to 22 min (WNIPU-20). In summary, in the same WPU coating, pigment content is the only factor that affects the drying. Adding appropriate pigments will decrease the drying time, but excessive amounts will increase it. An optimized amount of pigment is crucial for the drying/curing process in the coating system.

3.2. Morphology of the waterborne polyurethane coatings

Fig. S2 features microscopic photos of the commercial WPU coatings, while the rough surface of the synthetic WNIPU coating films prevented the acquisition of micrographs for this material. In the images, the pigment particles are represented in black, and the grey background represents the WPU coating matrix. For the WPU-0 sample, some dark lumpy substances are visible, which are the protruding polyurethanes formed during the curing process. With an increase in pigment content, the number of black spots noticeably increases, yet they remain well-distributed. This observation suggests that the pigments were effectively dispersed within the commercial WPU coating.

Figs. 2 and 3 show SEM images of the commercial WPU and the synthetic WNIPU coatings. In these images, the tiny white spots represent pigment particles, while the dark grey areas represent the coating matrix. As observed in Fig. 2 (a)-(e), with an increase in pigment content, a greater number of white spots appear without obvious agglomeration, some clusters appear, but the size remains relatively small, consistent with the micrographs (Fig. S2). Additionally, randomly distributed protrusions were observed in all films, corresponding to the dark lumpy substances observed in Fig. S2. Fig. 2 (f)-(j) displays cross-section micrographs of the commercial WPU coatings. The control sample (WPU-0) exhibited a smooth surface, and as the pigment content increased, more wrinkles appeared from WPU-1 to WPU-5. However, no significant change was observed with further increases in the pigment content.

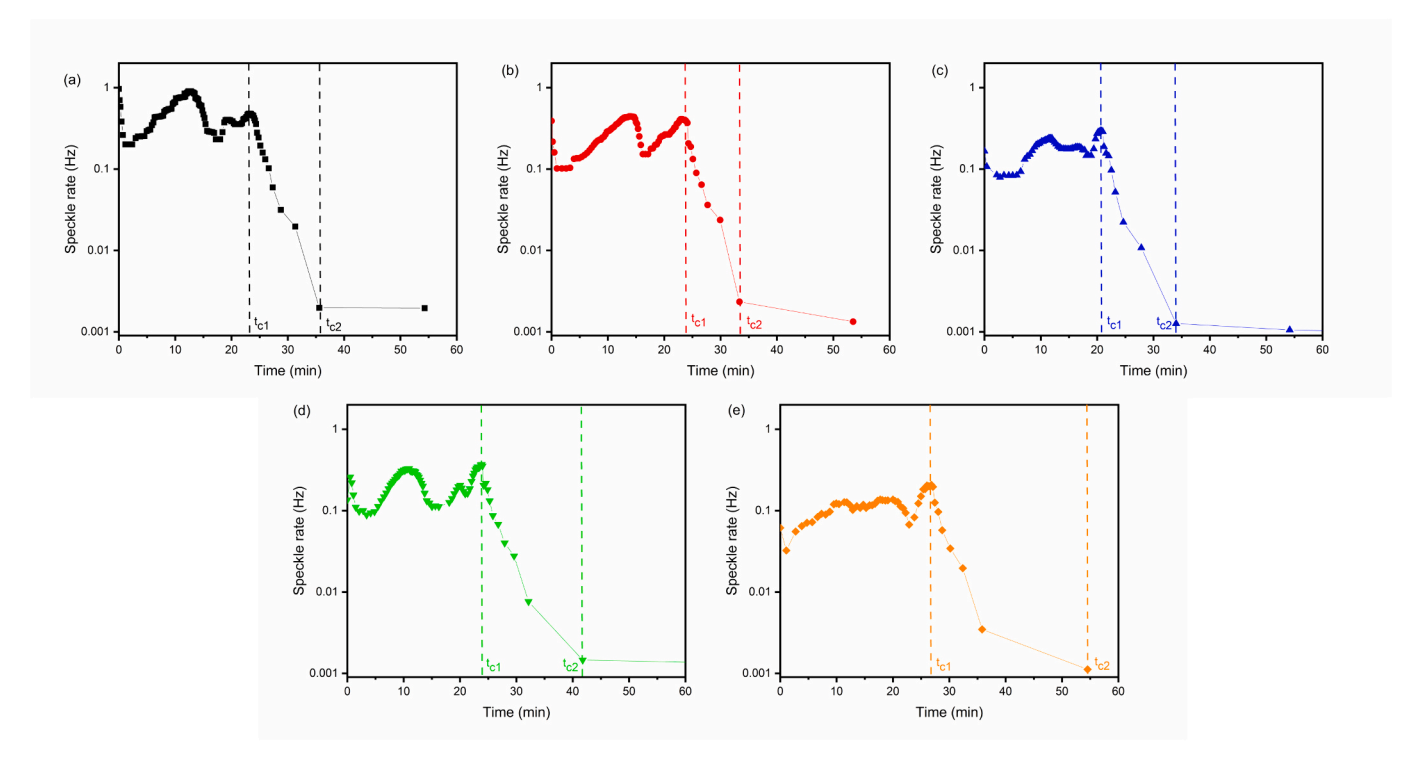


Fig. 1. Micro-dynamic of the commercial WPU coatings: (a) WPU-0, (b) WPU-1, (c) WPU-5, (d) WPU-10, and (e) WPU-20.

 Table 2

 Critical time during the waterborne coatings film formation process.

-	_	
	t _{c1} (min)	t _{c2} (min)
WPU-0	24	35
WPU-1	23	33
WPU-5	20	34
WPU-10	23	42
WPU-20	26	54
WNIPU-0	28	47
WNIPU-1	11	23
WNIPU-5	11	17
WNIPU-10	16	29
WNIPU-20	22	43

For the synthetic WNIPU coating films, as depicted in Fig. 3 (a)-(e), spherical structures appeared on the coating surface. As the pigment content increased, more spherical structures formed, accompanied by an increased presence of white spots, albeit at a lower concentration of

white spots compared to the commercial WPU coatings. These spherical structures in the synthetical WNIPU can diffuse light, resulting in a significantly lower gloss than that of the commercial WPU coatings (Gloss in Table 3) [28,29]. The formation of these spherical structures can be attributed to the heterogeneity during the curing process. Initially, the wet coating forms a drying top layer while the interior part remains wet. The mechanical mismatch between the dry surface and the wet interior, along with shrinkage due to water evaporation, causes deformation and the formation of spherical structures on the surface [30]. With a higher pigment content, the particles obstruct the movement path of interior water, leading to more pronounced surface deformation. In the cross-section of WNIPU-0 (Fig. 3 (f)), folds at the surface were observed, likely resulting from the constriction of water-borne polyurethane particles during the curing process [31].

Furthermore, with the incorporation of increasing amounts of pigments into the synthetic WNIPU, particle coagulation was observed at the bottom of the coatings, particularly for pigment content exceeding 5 wt% (Fig. 3 (h)-(j)). This phenomenon indicates poorer pigment

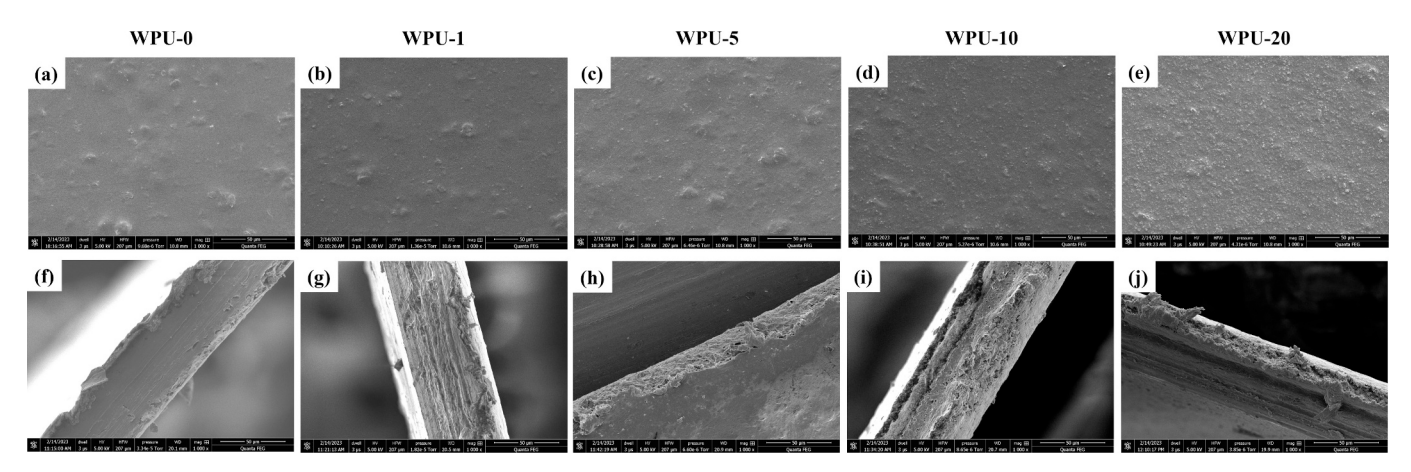


Fig. 2. SEM images of the commercial WPU coatings (a)-(e): top view and (f)-(j): cross-section. The scale bar in the SEM images is 50 µm.

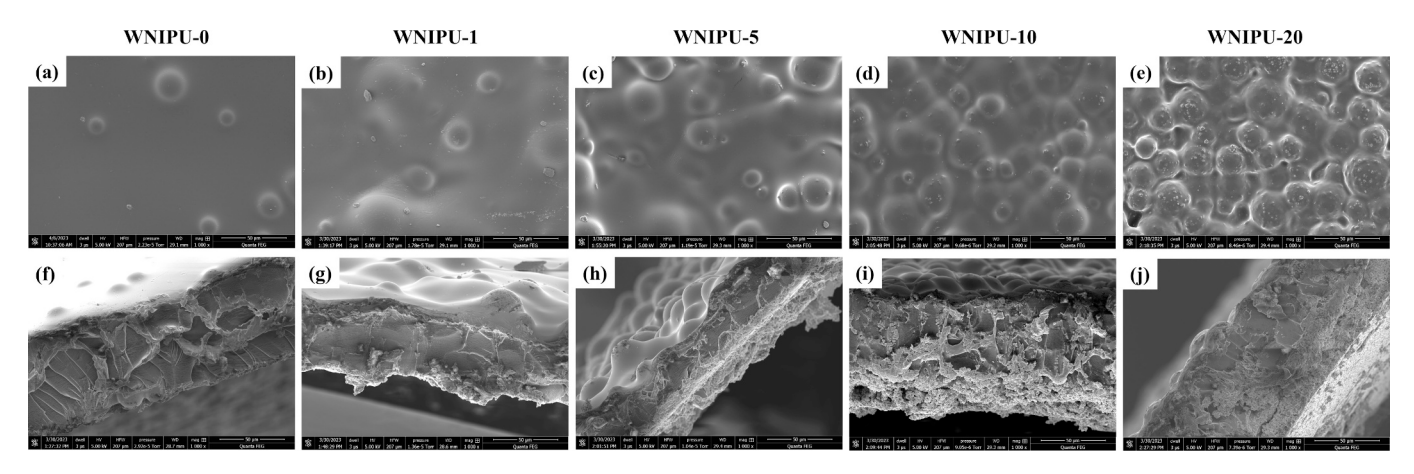


Fig. 3. SEM images of the synthetic WNIPU coatings (a)-(e): top view and (f)-(j): cross-section. The scale bar in the SEM images is 50 µm.

Table 3CIELAB values and gloss of pigmented waterborne polyurethane coatings.

	L	a*	b*	Gloss at 60°
WPU-0	68.35	0.20	0.93	52.42
WPU-1	34.31	0.09	-0.33	46.22
WPU-5	23.80	0.20	0.11	27.70
WPU-10	24.10	0.11	-0.05	25.44
WPU-20	24.13	0.10	0.01	14.8
WNIPU-0	66.05	-0.60	5.25	7.80
WNIPU-1	46.78	-0.44	2.86	3.30
WNIPU-5	27.18	0.17	-0.93	1.60
WNIPU-10	26.92	0.16	-1.13	1.74
WNIPU-20	24.44	0.26	-0.89	0.68

dispersion in the synthetic WNIPU than in the commercial WPU.

As shown in Fig. S3, the morphology of the pigment particles was observed by TEM. The particle size was approximately 0.9 μm with irregular shapes.

3.3. Gloss and color of the waterborne polyurethane coatings

Fig. 4 displays the digital photos of waterborne polyurethane films with different pigment concentrations. It is evident that as the pigment concentration increases, the coating films become darker. To quantitatively assess the color change, the CIELAB values and 60° gloss were recorded, which are presented in Table 3. Where L represents lightness, with values ranging from 0 to 100 indicating from black to white. The a^\star

and b* values, ranging from negative to positive, signify the shift from green to red and blue to yellow, respectively. The addition of NIR-reflective pigment resulted in a decrease in lightness for both commercial WPU and synthetic WNIPU coatings. The highest reduction occurred with 5 wt% of pigment. Further additions of pigments didn't markedly affect the lightness of the coatings. For the commercial WPU coatings, slight and irregular changes were observed in the a* and b* values with the addition of pigments. However, in the case of the synthetic WNIPU coatings, a* varied from -0.60 to 0.26, and b* varied from 5.25 to -0.89, indicating a shift in color from green to red and from yellow to blue, respectively.

With increasing content of pigments, the 60° gloss decreased from 52.42 to 14.8 for commercial WPU coatings and from 7.80 to 0.68 for synthetic WNIPU coatings. The gloss reduction suggests a negative impact of the pigment content on the light reflection of WPU coatings.

3.4. TGA of the waterborne polyurethane coating films

Fig. 5 displays the TGA curves of the waterborne polyurethane coating films with different pigment concentrations. In the case of commercial WPU (Fig. 5 (a)), the coatings initiated a dehydration process and experienced a significant weight loss after reaching 250 $^{\circ}$ C, due to the decomposition of polyurethane. The residue for the WPU-0 coating was virtually 0 wt%, indicating complete sample decomposition within this temperature range. Across the WPU-1 to WPU-20, the weight of the residue increased as the pigment concentration increased. The residue is the pigments left in the system after the thermal

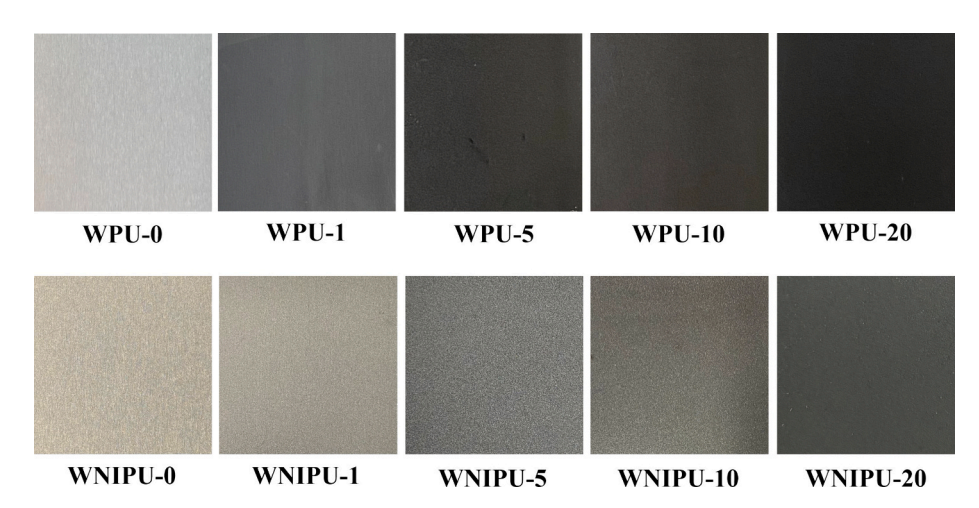


Fig. 4. Digital photos of the coatings: the commercial WPU with different pigment concentrations (top) and the synthetic WNIPU with different pigment concentrations (bottom).

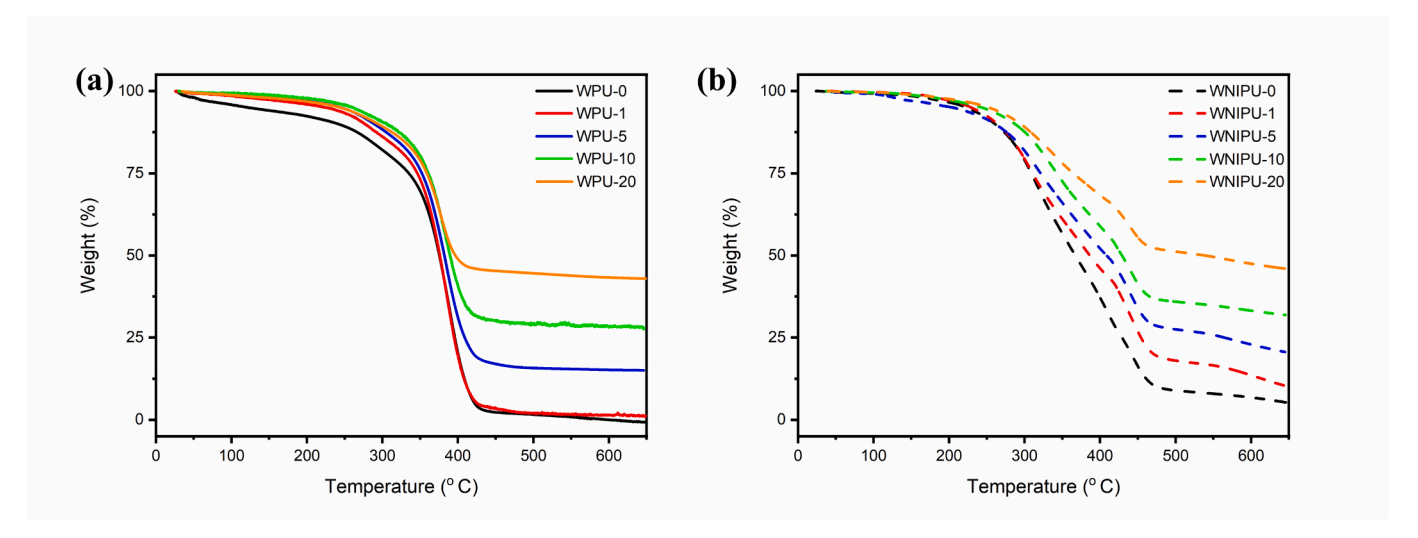


Fig. 5. TGA curves of (a) the commercial WPU coatings and (b) the synthetic WNIPU coatings.

decomposition of polyurethane and the residue weight follows the trend of the added pigments. The pigmented synthetic WNIPU coating behaved similarly to the pigmented commercial WPU coating, as depicted in Fig. 5 (b).

3.5. Viscoelastic properties

The viscoelastic properties of the pigmented waterborne polyurethane coatings were evaluated by DMTA, and Fig. 6 presents the curves of storage modulus and tanô as a function of temperature.

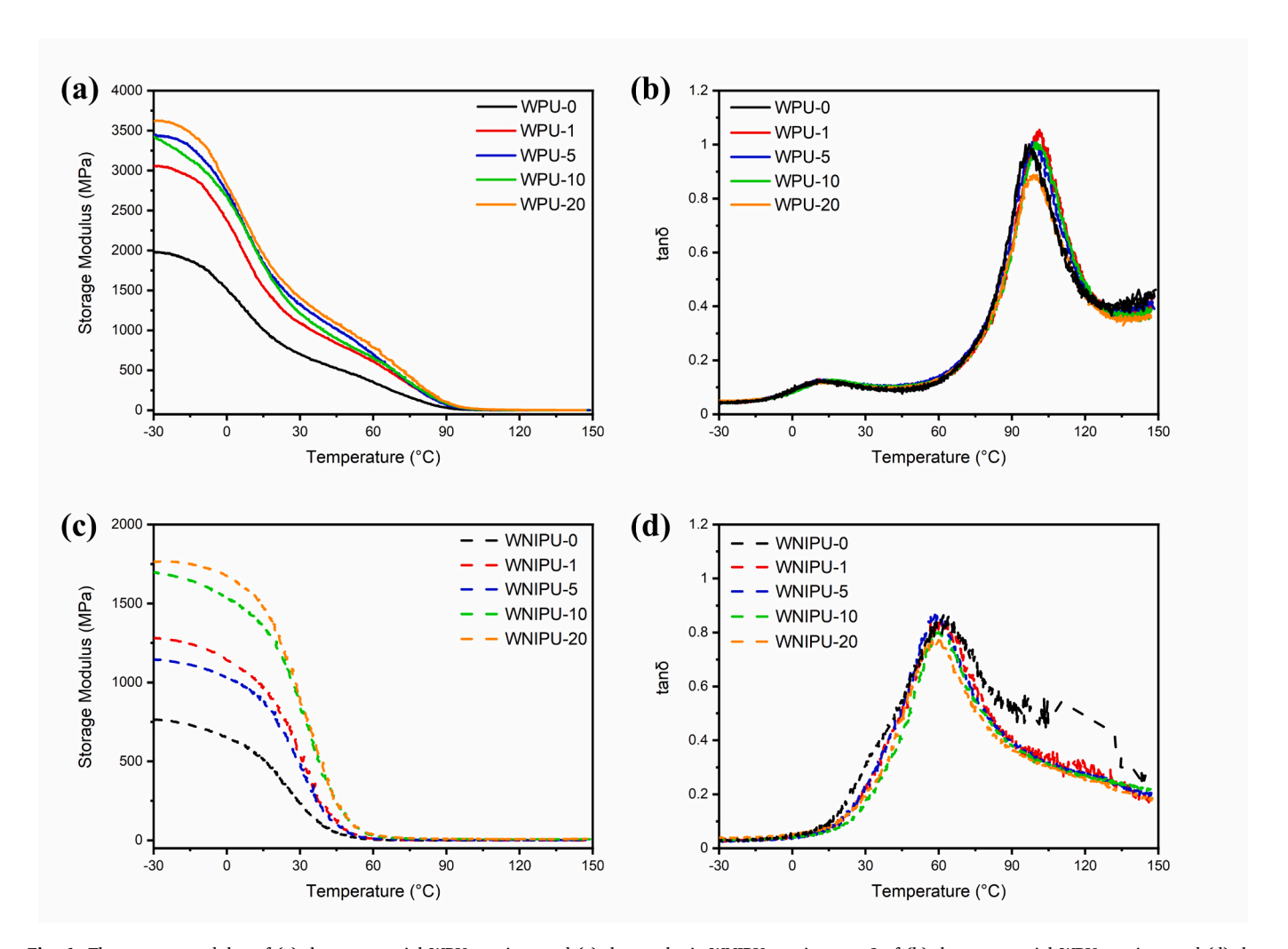


Fig. 6. The storage modulus of (a) the commercial WPU coatings and (c) the synthetic WNIPU coatings. $tan\delta$ of (b) the commercial WPU coatings and (d) the synthetic WNIPU coatings.

Additionally, Table 4 lists the T_g , storage modulus at $T_g + 40$ °C, and cross-link density (ν_e). T_g was determined at the temperature corresponding to the maximum tan δ . The cross-link density was calculated using Eq. (1) [32]:

$$\nu_{\rm e} E/3RT$$
 (1)

where E' is the storage modulus in the rubbery plateau, R is the gas constant, and T is the temperature in Kelvin.

From Fig. 6 (a) and (c), it is evident that the addition of pigments results in higher E' for pigmented coatings compared to non-pigmented coatings. This phenomenon can be attributed to the reinforcement provided by the inorganic pigment, possibly due to polymer-pigment interactions. Moreover, in the rubbery region, an increase in the amount of pigments leads to a higher E', also indicating an increased cross-link density in the WPU coatings. In Table 4, the cross-link density varied from 53.76 to 203.3 mol/m³ for the commercial WPU and from 11.76 to 987.24 mol/m³ for the synthetic WNIPU. This trend aligns with a previous report, which found that increasing pigment content correlates with the increased E' in waterborne basecoat [33]. Regarding the tanδ curves (Fig. 6 (b)), commercial WPU coatings exhibited two T_g values, indicating a microphase separation between the hard and soft segments of PU [34]. In contrast, the synthetic WNIPU coatings displayed only one Tg peak (Fig. 6 (d)), suggesting compatibility between the soft and hard segments in this system [35]. Notably, the addition of pigment did not significantly affect the $T_{\rm g}$ values. The observation can be explained by the interplay of two opposing factors: (1) a decrease in T_g due to the increased polymer mobility on the surface of inorganic pigment particles; and (2) an increase in Tg due to the hindrance effect of pigment particles [36]. In this study, it appears that these two factors counterbalanced each other, resulting in no significant change in Tg.

3.6. Tensile results

The results of the tensile test for pigmented WPU and WNIPU coatings are presented in Fig. 7. From the results, as the increasing of pigment content, the coatings exhibited higher tensile stress, lower elongation-at-break, and higher Young's modulus. The increase in tensile stress and Young's modulus can be attributed to the higher crosslink density resulting from the interaction between the polymer and pigment particles, as indicated by the DMTA results. Additionally, the inorganic pigment particles possess higher stiffness than the polymer, which contributes to the enhancement of tensile stress and Young's modulus [37,38].

3.7. Thermal insulation behavior

The NIR reflection efficiency of the pigmented waterborne polyurethane coatings was assessed through a temperature test to mimic the roof coating of a building. The coating panels were affixed to foam boxes, with a 250 W infrared lamp (Philips) positioned 30 cm away from the coating panels, as illustrated in Scheme 2. The temperatures of both the front and back sides of the panels were recorded by the thermal

Table 4Viscoelastic properties of waterborne polyurethane coatings.

	T_{g1} (°C)	T _{g2} (°C)	E' at $T_g + 40^{\circ}\text{C}$ (MPa)	$\nu_{\rm e}~({\rm mol/m^3})$
WPU-0	13	97	0.55	53.76
WPU-1	12	100	0.75	72.78
WPU-5	13	99	0.94	91.44
WPU-10	15	99	1.18	114.50
WPU-20	13	99	2.09	203.31
WNIPU-0	62	_	0.11	11.76
WNIPU-1	61	_	0.34	36.45
WNIPU-5	58	_	2.27	245.31
WNIPU-10	60	_	7.57	813.68
WNIPU-20	59	_	9.16	987.24

camera (FLIR TG165-X) and listed in Table 5.

Thermal images captured by the thermal camera are presented in Figs. S4 and S5. For this investigation, the coatings with 1 wt% carbon black were selected as the control groups of waterborne polyurethane coatings with 1 wt% NIR-reflective pigment. The results showed that both WPU-1 and WNIPU-1 exhibited lower temperatures and higher temperature differences compared to the control groups, indicating better thermal insulation performance with NIR-reflective pigment. This is due to the higher NIR reflectance of copper chromite pigment compared to carbon black, as noted in a previous study [39]. Additionally, copper chromite spinel has high reflectance at the 1000 nm and 1500 nm peaks in the NIR region, contributing to its NIR-reflective property [40,41]. However, as the pigment content increased, both the temperatures in front of and behind the panels increased, indicating a decrease in NIR reflectance. A similar phenomenon was observed in other research, where increasing copper chromite black pigment resulted in reduced NIR reflectance [42]. In summary, adding NIR-reflective pigments can provide thermal insulation for the waterborne polyurethane coatings compared to carbon black, but the content should be carefully determined to achieve the desired thermal insulation behavior.

4. Conclusion

In this study, a commercial black NIR-reflective pigment was added to commercial WPU and synthetic WNIPU coatings to explore the property-processing relationship of the pigments in waterborne coatings. The following conclusions can be dawn:

- The addition of pigment could initially shorten the drying time but with higher pigment content, the overall drying time was prolonged due to the rapid drying of the top layer, which hinders internal water evaporation.
- The addition of pigment could hinder water evaporation, causing pronounced shrinkage and spherical structures on synthetic WNIPU surfaces.
- Incorporating more NIR-reflective pigment led to enhanced storage modulus and crosslink density, along with strengthening tensile stress and Young's modulus due to the pigment's stiffness.
- Higher pigment content reduced the gloss of waterborne polyurethane coatings.
- In comparison to carbon black-pigmented coating, NIR-pigmented coatings showed thermal insulation behavior. The 5 wt% of black NIR pigment in WPU and 1 wt% in WNIPU showed the best balance of drying time, color, mechanical properties, and thermal insulation behavior.

Finally, the addition of pigment introduces complexity in the film formation of waterborne coatings and influences the general coating properties. Therefore, careful consideration of pigment content is crucial when formulating waterborne coatings.

CRediT authorship contribution statement

Zichen Ling: Writing – review & editing, Writing – original draft, Validation, Methodology, Investigation, Formal analysis, Conceptualization. **Qixin Zhou:** Writing – review & editing, Writing – original draft, Validation, Supervision, Project administration, Funding acquisition.

Declaration of competing interest

The authors declare that they have no known competing financial interests or personal relationships that could have appeared to influence the work reported in this paper.

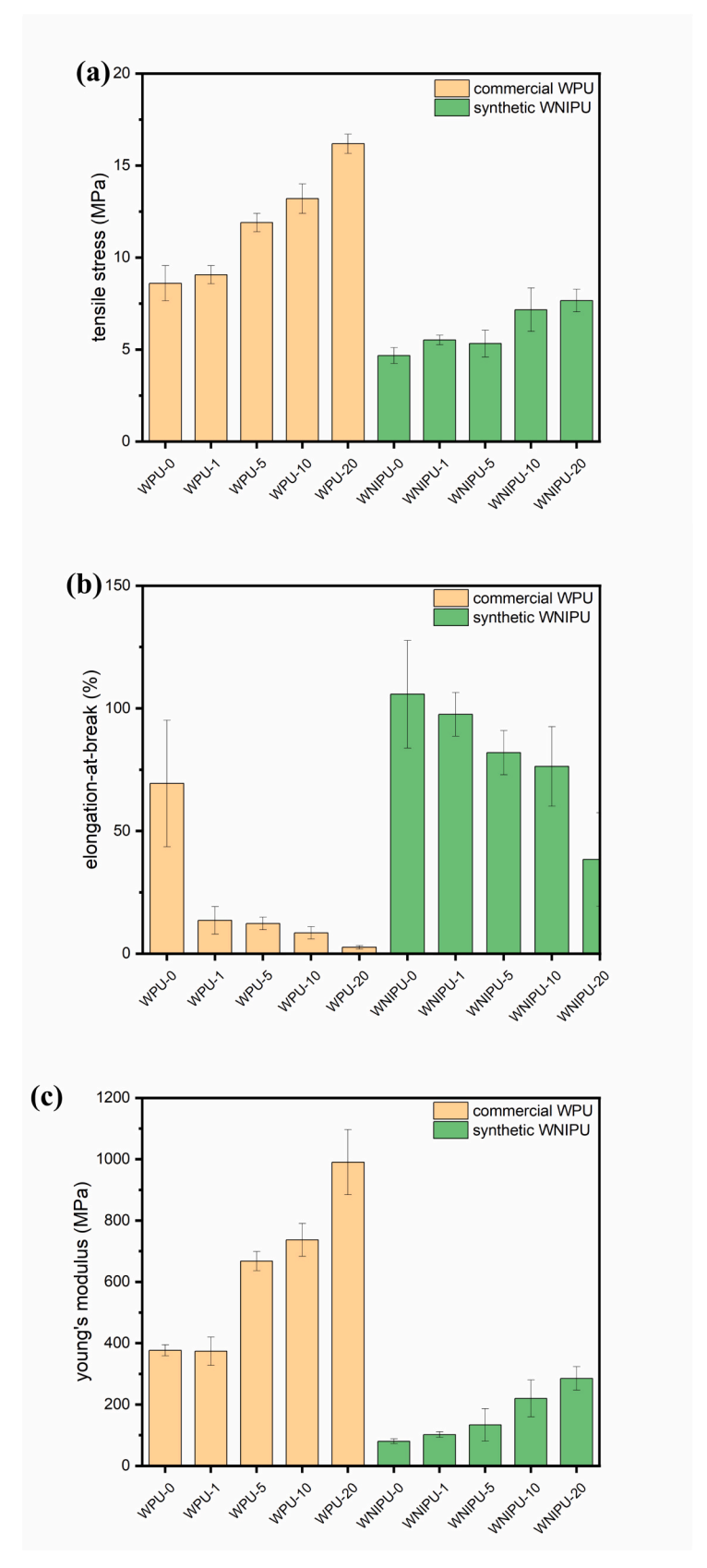
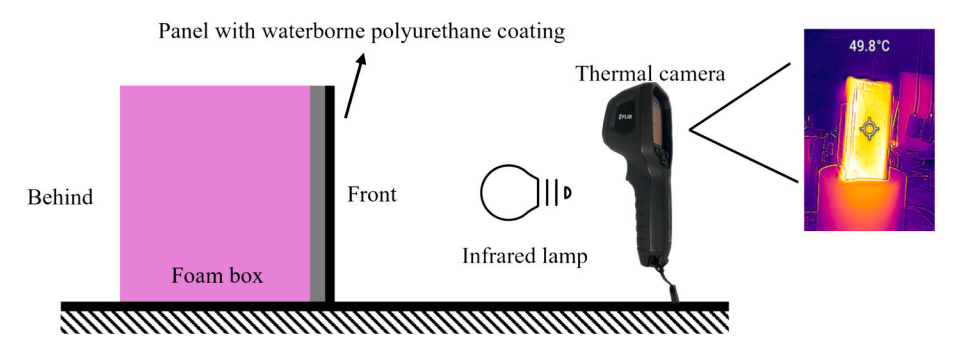


Fig. 7. (a) Tensile stress, (b) elongation-at-break, and (c) Young's modulus of commercial WPU and synthetic WNIPU coatings.



Scheme 2. Experimental setup for the temperature test.

Table 5Temperatures on the surfaces of the waterborne polyurethane coatings.

Sample	Temperature in front of the panel	Temperature behind the panel	Temperature difference
WPU + 1 % CB	49.8	49.5	0.3
WPU-1	43.5	41.3	2.2
WPU-5	50.4	47.0	3.4
WPU-10	52.6	49.0	3.6
WPU-20	55.7	49.2	6.5
WNIPU+1 %	47.9	47.1	0.8
CB			
WNIPU-1	44.3	41.4	2.9
WNIPU-5	50.1	47.2	2.9
WNIPU-10	52.2	49.0	3.2
WNIPU-20	53.0	49.7	3.3

Data availability

Data will be made available on request.

Acknowledgment

The authors acknowledge the support from the U.S. National Science Foundation (NSF CAREER Award, #1943860). The SEM and TEM data were tested in the Characterization Facility of the Liquid Crystal Institute at Kent State University. The assistance of Dr. Min Gao to provide TEM and SEM training is appreciated. The MS-DWS data were obtained from FORMULACTION Scientific Instruments. The assistance of Floriane Charpentier in providing MS-DWS analysis is appreciated.

Appendix A. Supplementary data

The supporting information is available. This information includes micro-dynamic of the synthetical WNIPU coatings, microscopic images of commercial WPU coatings, a TEM image of the NIR-reflective pigment, and thermal images of commercial WPU coatings and WNIPU coatings. Supplementary data to this article can be found online at doi:https://doi.org/10.1016/j.porgcoat.2024.108678.

References

- [1] P. Anastas, N. Eghbali, Green chemistry: principles and practice, Chem. Soc. Rev. 39 (2009) 301–312, https://doi.org/10.1039/B918763B.
- [2] M.F. Cunningham, J.D. Campbell, Z. Fu, J. Bohling, J.G. Leroux, W. Mabee, T. Robert, Future green chemistry and sustainability needs in polymeric coatings, Green Chem. 21 (2019) 4919–4926, https://doi.org/10.1039/C9GC02462J.
- [3] V. Fetisov, A.M. Gonopolsky, H. Davardoost, A.R. Ghanbari, A.H. Mohammadi, Regulation and impact of VOC and CO2 emissions on low-carbon energy systems resilient to climate change: a case study on an environmental issue in the oil and gas industry, Energy Sci. Eng. 11 (2023) 1516–1535, https://doi.org/10.1002/ ESF3 1383
- [4] Waterborne Coatings Market Size & Forecast [Latest], (n.d.). https://www.market sandmarkets.com/Market-Reports/waterborne-waterbased-coatings-market -205422792.html (accessed September 5, 2023).

- [5] X. Wang, B. Mu, Z. Zhang, A. Wang, Insights into halloysite or kaolin role of BiVO4 hybrid pigments for applications in polymer matrix and surface coating, Compos B Eng 174 (2019) 107035, https://doi.org/10.1016/J.COMPOSITESB.2019.107035.
- [6] P.K. Thejus, K.V. Krishnapriya, K.G. Nishanth, A cost-effective intense blue colour inorganic pigment for multifunctional cool roof and anticorrosive coatings, Sol. Energy Mater. Sol. Cells 219 (2021) 110778, https://doi.org/10.1016/J. SOLMAT.2020.110778.
- [7] R.R. Ramesh, S. Murali, M.A. Javid, R.R. Jonnalagadda, Robust synthesis of water stable ciprofloxacin functionalized hybrid metal-organic antimicrobial pigments for coating applications, Dyes Pigments 218 (2023) 111499, https://doi.org/ 10.1016/J.DYEPIG.2023.111499.
- [8] S. Sultan, K. Kareem, L. He, Synthesis, characterization and resistant performance of α-Fe2O3@SiO2 composite as pigment protective coatings, Surf. Coat. Technol. 300 (2016) 42–49, https://doi.org/10.1016/J.SURFCOAT.2016.05.010.
- [9] A. Kalendová, I. Sapurina, J. Stejskal, D. Veselý, Anticorrosion properties of polyaniline-coated pigments in organic coatings, Corros. Sci. 50 (2008) 3549–3560, https://doi.org/10.1016/J.CORSCI.2008.08.044.
- [10] B. Sarkodie, C. Acheampong, B. Asinyo, X. Zhang, B. Tawiah, Characteristics of pigments, modification, and their functionalities, Color. Res. Appl. 44 (2019) 396–410, https://doi.org/10.1002/COL.22359.
- [11] N. Xie, H. Li, A. Abdelhady, J. Harvey, Laboratorial investigation on optical and thermal properties of cool pavement nano-coatings for urban heat island mitigation, Build. Environ. 147 (2019) 231–240, https://doi.org/10.1016/J. BUILDENV.2018.10.017
- [12] S. Zhuo, W. Zhou, P. Fang, J. Ye, H. Luo, H. Li, C. Wu, W. Chen, Y. Liu, Cost-effective pearlescent pigments with high near-infrared reflectance and outstanding energy-saving ability for mitigating urban heat island effect, Appl. Energy 353 (2024) 122051, https://doi.org/10.1016/J.APENERGY.2023.122051.
- [13] L. Liu, A. Han, M. Ye, W. Feng, The evaluation of thermal performance of cool coatings colored with high near-infrared reflective nano-brown inorganic pigments: magnesium doped ZnFe2O4 compounds, Sol. Energy 113 (2015) 48–56, https://doi.org/10.1016/J.SOLENER.2014.12.034.
- [14] A. Rosati, M. Fedel, S. Rossi, NIR reflective pigments for cool roof applications: a comprehensive review, J. Clean. Prod. 313 (2021) 127826, https://doi.org/ 10.1016/J.JCLEPRO.2021.127826.
- [15] J. Zou, Y. Chen, H. Lin, Facile fabrication of cool yellow pigment with enhanced NIR reflectance by tailoring oxygen defects and its application in energy-saving building, Ceram. Int. 49 (2023) 10756–10764, https://doi.org/10.1016/J. CERAMINT.2022.11.268.
- [16] D.S. Parker, S.F. Barkaszi, Roof solar reflectance and cooling energy use: field research results from Florida, Energ. Buildings 25 (1997) 105–115, https://doi. org/10.1016/S0378-7788(96)01000-6.
- [17] Z. You, M. Zhang, J. Wang, W. Pei, A black near-infrared reflective coating based on nano-technology, Energ. Buildings 205 (2019) 109523, https://doi.org/ 10.1016/J.ENBUILD.2019.109523.
- [18] F. Martini, P. Minei, M. Lessi, L. Contiero, S. Borsacchi, G. Ruggeri, M. Geppi, F. Bellina, A. Pucci, Structural order and NIR reflective properties of perylene bisimide pigments: experimental evidences from a combined multi-technique study, Dyes Pigments 179 (2020) 108401, https://doi.org/10.1016/J. DYEPIG.2020.108401.
- [19] A. Wegmann, Chemical resistance of waterborne epoxy/amine coatings, Prog. Org. Coat. 32 (1997) 231–239, https://doi.org/10.1016/S0300-9440(97)00062-3.
- [20] A. Overbeek, F. Bückmann, E. Martin, P. Steenwinkel, T. Annable, New generation decorative paint technology, Prog. Org. Coat. 48 (2003) 125–139, https://doi.org/ 10.1016/S0300-9440(03)00101-2.
- [21] S.T. Eckersley, A. Rudin, Film formation of acrylic copolymer Latices: a model of stage II film formation, ACS Symp. Ser. 648 (1996) 18, https://doi.org/10.1021/ BK-1996-0648.CH001.
- [22] Q. Nawaz, Y. Rharbi, Various modes of void closure during dry sintering of close-packed nanoparticles, Langmuir 26 (2010) 1226–1231, https://doi.org/10.1021/LA902381B/SUPPL_FILE/LA902381B_SI_001.PDF.
- [23] H.M. Van Der Kooij, G.T. Van De Kerkhof, J. Sprakel, A mechanistic view of drying suspension droplets, Soft Matter 12 (2016) 2858–2867, https://doi.org/10.1039/ C5SM02406D
- [24] Z. Ling, C. Zhang, Q. Zhou, Synthesis and characterization of 1 K waterborne non-isocyanate polyurethane epoxy hybrid coating, Prog. Org. Coat. 169 (2022) 106915, https://doi.org/10.1016/J.PORGCOAT.2022.106915.

- [25] A. Brun, H. Dihang, L. Brunel, Film formation of coatings studied by diffusing-wave spectroscopy, Prog. Org. Coat. 61 (2008) 181–191, https://doi.org/10.1016/J. PORGCOAT.2007.09.041.
- [26] V. Viasnoff, F. Lequeux, D.J. Pine, Multispeckle diffusing-wave spectroscopy: a tool to study slow relaxation and time-dependent dynamics, Rev. Sci. Instrum. 73 (2002) 2336–2344, https://doi.org/10.1063/1.1476699.
- [27] I. Giraud, E. Dantras, A. Brun, H. Dihang, L. Brunel, A. Bernès, G. Meunier, C. Lacabanne, Film formation analysis by diffusive wave spectroscopy, Prog. Org. Coat. 64 (2009) 515–519, https://doi.org/10.1016/J.PORGCOAT.2008.07.017.
- [28] J. Zhu, H. Huang, X. Peng, Preparation and characterization of antiglare waterborne polyurethane, RSC Adv. 6 (2016) 102368–102372, https://doi.org/ 10.1039/f6B.423989G
- [29] J. Li, W. Zheng, W. Zeng, D. Zhang, X. Peng, Structure, properties and application of a novel low-glossed waterborne polyurethane, Appl. Surf. Sci. 307 (2014) 255–262, https://doi.org/10.1016/J.APSUSC.2014.04.022.
- [30] Q. Yong, H. Pang, B. Liao, W. Mo, F. Huang, H. Huang, Y. Zhao, Preparation and characterization of low gloss aqueous coating via forming self-roughed surface based on waterborne polyurethane acrylate hybrid emulsion, Prog. Org. Coat. 115 (2018) 18–26. https://doi.org/10.1016/J.PORGCOAT.2017.10.024.
- [31] X. Cao, X. Ge, H. Chen, W. Li, Effects of trimethylol propane and AAS salt on properties of waterborne polyurethane with low gloss, Prog. Org. Coat. 107 (2017) 5–13, https://doi.org/10.1016/J.PORGCOAT.2017.02.021.
- [32] L.W. Hill, Calculation of crosslink density in short chain networks, Prog. Org. Coat. 31 (1997) 235–243, https://doi.org/10.1016/S0300-9440(97)00081-7.
- [33] W. Schlesing, M. Buhk, M. Osterhold, Dynamic mechanical analysis in coatings industry, Prog. Org. Coat. 49 (2004) 197–208, https://doi.org/10.1016/J. PORGCOAT.2003.09.009.
- [34] B. Fernándezfernández-D'arlas, J.A. Ramos, A. Saralegi, M. Corcuera, I. Aki Mondragon, A. Eceiza, Molecular Engineering of Elastic and Strong Supertough Polyurethanes, 2012, https://doi.org/10.1021/ma300397e.

- [35] K. Jiang, W. Chen, X. Liu, Y. Wang, D. Han, Q. Zhang, Effect of bio-based polyols and chain extender on the microphase separation structure, mechanical properties and morphology of rigid polyurethane foams, Eur. Polym. J. 179 (2022) 111572, https://doi.org/10.1016/J.EURPOLYMJ.2022.111572.
- [36] T. Gao, E. Maya-Visuet, Z. He, H. Castaneda-Lopez, I.J. Zvonkina, M.D. Soucek, Effect of pigmentation on polyurethane/polysiloxane hybrid coatings, J. Appl. Polym. Sci. 133 (2016) 42947, https://doi.org/10.1002/APP.42947.
- [37] S.Y. Fu, X.Q. Feng, B. Lauke, Y.W. Mai, Effects of particle size, particle/matrix interface adhesion and particle loading on mechanical properties of particulate-polymer composites, Compos B Eng 39 (2008) 933–961, https://doi. org/10.1016/J.COMPOSITESB.2008.01.002.
- [38] J. Miklečić, S.L. Blagojević, M. Petrič, V. Jirouš-Rajković, Influence of TiO2 and ZnO nanoparticles on properties of waterborne polyacrylate coating exposed to outdoor conditions, Prog. Org. Coat. 89 (2015) 67–74, https://doi.org/10.1016/J. PORGCOAT 2015 07 016
- [39] J. Qin, J. Song, J. Qu, X. Xue, W. Zhang, Z. Song, Y. Shi, L. Jiang, J. Li, T. Zhang, The methods for creating building energy efficient cool black coatings, Energ. Buildings 84 (2014) 308–315, https://doi.org/10.1016/J.ENBUILD.2014.08.022.
- [40] Q. Geng, X. Zhao, X. Gao, S. Yang, G. Liu, Low-temperature combustion synthesis of CuCr 2O 4 spinel powder for spectrally selective paints, J Solgel Sci Technol 61 (2012) 281–288, https://doi.org/10.1007/S10971-011-2625-2/FIGURES/8.
- [41] E. Pakzad, Z. Ranjbar, M. Ghahari, Synthesized of octahedral cupper chromite spinel for spectrally selective absorber (SSA) coatings, Prog. Org. Coat. 132 (2019) 21–28, https://doi.org/10.1016/J.PORGCOAT.2019.03.027.
- [42] X. Xue, J. Qin, J. Song, J. Qu, Y. Shi, W. Zhang, Z. Song, L. Jiang, J. Li, H. Guo, T. Zhang, The methods for creating energy efficient cool gray building coatings—part I: preparation from white and black pigments, Sol. Energy Mater. Sol. Cells 130 (2014) 587–598, https://doi.org/10.1016/J.SOLMAT.2014.07.044.